IEEE Access
Multidisciplinary | Rapid Review | Open Access Journal

Received August 6, 2021, accepted August 22, 2021, date of publication September 2, 2021, date of current version September 10, 2021.

Digital Object Identifier 10.1109/ACCESS.2021.3109568

Similarity Analysis Between a Nonmodel-Based Disturbance Observer and a Time-Delayed Controller for Robot Manipulators in Cartesian Space

SEUL JUNG, (Member, IEEE), AND JOON WOO LEE
Department of Mechatronics Engineering, Chungnam National University, Daejeon 34134, South Korea

Corresponding author: Seul Jung (jungs@cnu.ac.kr)

This work was supported in part by the NRF of Korea, in 2019 under Grant 2017K1A3A1A68072072 and Grant 2019R1I1A3A01062567.

ABSTRACT Disturbance observer (DOB) techniques are effective and practical methods for rejecting disturbances in motion control applications. Nonlinear DOBs that are based on dynamic models are employed to apply the robust control technique to robot manipulators to improve position tracking performances. Time-delayed control techniques are also effective methods for addressing uncertainties in robot manipulators. Recent research results have demonstrated that both schemes are robust in compensating for highly nonlinear uncertainties in robot dynamics. The objective of this paper is to demonstrate the structural equivalence between a nonlinear disturbance observer and a time-delayed controller (TDC) under the nonmodel-based control framework of robot manipulators. In addition, a Cartesian TDC for robot manipulators is implemented and its stability is analyzed. The effects on the tracking performance in terms of sampling times, inertia values, and torque constants of the Cartesian TDC are compared and analyzed for a robot manipulator that follows a circular trajectory by both numerical and empirical investigations.

INDEX TERMS Disturbance observers, time-delayed control, equivalent structure, stability, robot manipulators.

I. INTRODUCTION

Disturbance observer is a major control scheme for rejecting uncertainties of internal nonmodel dynamics and external disturbances in motion control applications [1]. Linear disturbance observers(DOBs) are implemented with inverse models of linear systems and Q filter design [2]. Nonlinear DOBs can be implemented with dynamic models of the target system to realize the inverse dynamics control for nonlinear systems such as robot manipulators [3]–[8]. Thus, the accuracy of the dynamic models of the system is the most important issue for DOB implementation.

However, modelling dynamical systems is not easy, and the accuracy of modelling is uncertain. The exact modeling of dynamical systems is impossible since there are many nonmodeled dynamic components such as unknown payloads, friction, stiction, back lash, and hysteresis. Since robot manipulators are highly nonlinear and multi-input multi-output systems, accurate positioning control with dynamic model compensation is challenging. This leads to the development of control algorithms for addressing modeling uncertainties, along with completely unknown dynamics.

Decentralized adaptive sliding mode control with disturbance observers for robot manipulators was proposed [9]. Intelligent techniques are promising candidates for addressing nonmodel dynamics. Neural network control schemes for learning the inverse dynamics of robot manipulators have been presented [10], [11]. Online learning and control were conducted to learn a robot system by defining training signals to cancel out uncertainties [12]. Neural network-based learning has the substantial advantage of a simple learning and control structure, but it requires fast and massively parallel computing to realize online learning and control [13]–[15]. Fuzzy control methods have been presented for robustly addressing changes in systems [16]–[18]. Fuzzy control shows advantages in interpreting human expressions, but establishing optimal rules that satisfy the control performance requirements is difficult and requires a time-consuming process.

The associate editor coordinating the review of this manuscript and approving it for publication was Zhiguang Feng.

Therefore, in the nonmodel-based control framework for robot manipulators, the time-delayed control (TDC) is a promising candidate for the robust control performance due to its simplicity and robustness [19], [20]. TDC uses the previously sampled control information of the acceleration measurement and the inertia matrix [21]. Consequently, a fast sampling time is required, which affects the performance and the stability of the system in the linear system analysis.

However, the stability of TDC for the nonlinear systems such as robot manipulators can be analyzed differently from that in linear cases. The stability issues of TDC have been addressed and the stability was found to depend upon the inertia matrices of the robot manipulators [15], [22]. In consideration of the stability issues in TDC, sliding mode control with TDC was proposed, and adaptive techniques were applied to TDC for robot manipulators to mitigate the disadvantages of the TDC scheme [23]–[26].

The objective of this paper is to prove that the TDC structure for robot manipulators becomes equivalent the nonmodel-based disturbance observer structure. When nonlinear model-based DOBs are implemented in real systems, computational time delays for calculating the inverse dynamic models are required. Since the concept is the same for the nonlinear nonmodel-based DOB design with computational time delays, the design structure is exactly same as the TDC structure. Eventually, the nonlinear nonmodel-based DOB becomes TDC.

In the framework of the Cartesian space control of robot manipulators, TDC is designed, and its stability is analyzed. Extensive simulation studies of tracking the circular trajectory of a three-link robot manipulator are performed to evaluate the robustness of the control performance by TDC. Sampling time issues are addressed through simulation studies. The selection of suitable torque constants for leveling the Cartesian space and the joint space is suggested. The stability issue of selecting the inertia value for the constant inertia matrix is addressed through extensive simulation studies.

Finally, empirical studies are conducted, and the results support the outperformance of the TDC scheme.

II. ROBOT DYNAMICS

The dynamics of an n joint robot manipulator with external disturbance and internal nonmodel dynamics is described as

$$D(q)\ddot{q} + C(q,\dot{q}) + G(q) + \tau_u = \tau + \tau_{dis}, \tag{1}$$

where $D(q)$ is the n x n inertia matrix, $C(q,\dot{q})$ is the n x 1 Coriolis and centrifugal torque vector, $G(q)$ is the n x 1 gravity force vector, $q(t)$ is the n x 1 joint angle vector, $\dot{q}(t)$ is the n x 1 joint angular velocity vector, $\ddot{q}(t)$ is the n x 1 joint angular acceleration vector, $\tau_u(t)$ is the n x 1 other nonmodeled torque vector, $\tau_{dis}(t)$ is the n x 1 external disturbance, and $\tau(t)$ is the n x 1 input torque vector.

The Jacobian relationship is expressed as

$$\dot{X}(t) = J(q)\dot{q}(t), \tag{2}$$

where $J(q)$ is the n x n Jacobian matrix. The Cartesian dynamics equation is established by using (2).

$$D^*(t)\ddot{X}(t) + C^*(t) + G^*(t) + F_u(t) = F(t) + F_{dis}(t), \tag{3}$$

where $D^*(t) = J^{-T}D(q)J^{-1}$ is the n x n Cartesian inertia matrix, $C^*(t) = -J^{-T}D(q)J^{-1}\dot{J}J^{-1}\dot{X} + J^{-T}C(q,\dot{q})$ is the n x 1 Cartesian Coriolis and centrifugal force vector, $G^*(t) = J^{-T}G(q)$ is the n x 1 Cartesian gravity force vector, $X(t)$ is the n x 1 position vector, $\dot{X}(t)$ is the n x 1 linear velocity vector, $\ddot{X}(t)$ is the n x 1 linear acceleration vector, $F_u(t)$ is the n x 1 nonmodel force vector, $F_{dis}(t)$ is the n x 1 external disturbance vector, and $F(t)$ is the n x 1 input force vector.

For simplicity, (3) can be reformulated as

$$D^*(t)\ddot{X}(t) + H^*(t) + F_u(t) = F(t) + F_{dis}(t), \tag{4}$$

where $H^*(t) = C^*(t) + G^*(t)$, which can be modelled.

III. DISTURBANCE OBSERVER

Here disturbance observers are designed for the Cartesian position control of robot manipulators.

A. MODEL-BASED DISTURBANCE OBSERVER

The Cartesian dynamic model with uncertainty is expressed as

$$D^*(t)\ddot{X}(t) + H^*(t) + F_{ud}(t) = F(t) \tag{5}$$

where $F_{ud}(t) = F_u(t) - F_{dis}(t)$ is the uncertainty. The Cartesian control input $V(t)$ is defined as a PD-typed control as

$$V(t) = \ddot{X}_d(t) + K_D\dot{e}(t) + K_P e(t), \tag{6}$$

where $X_d(t)$ is the desired trajectory, $e(t) = X_d(t) - X(t)$ and K_D, K_P are controller gain matrices.

The control law with a delayed disturbance estimate becomes

$$F(t) = \bar{F}(t) - \hat{F}_{ud}(t - T), \tag{7}$$

where $\hat{F}_{ud}(t - T)$ is the delayed estimate of the disturbance that is due to the model calculation time, namely the sampling time T and $\bar{F}(t)$ is the model-based control law, which is defined as

$$\bar{F}(t) = \hat{D}^*(t)V(t) + \hat{H}^*(t), \tag{8}$$

where $\hat{D}^*(t), \hat{H}^*(t)$ are estimates of $D^*(t), H^*(t)$, respectively.

The disturbance with nonmodeled dynamics is defined from Fig. 1 as

$$F_{ud}(t) = \tilde{F}(t) - F(t), \tag{9}$$

where $\tilde{F}(t)$ is the actual control input force including external disturbance $F_{ud}(t)$, which is not available. Since the disturbance cannot be estimated directly, we use the dynamic models to estimate the disturbance indirectly as

$$\hat{F}_{ud}(t) = F_{est}(t) - F(t), \tag{10}$$

where $F_{est}(t)$ is the estimated dynamic model, which is expressed as

$$F_{est}(t) = \hat{D}^*(t)\ddot{X}(t) + \hat{H}^*(t). \tag{11}$$

where $\ddot{X}(t)$ is the acceleration signal that includes the disturbance information. In practice, the acceleration signals are measured by sensors or can be estimated by suitable filters.

Substituting (11) into (10) yields the disturbance estimate

$$\hat{F}_{ud}(t) = \hat{D}^*(t)\ddot{X}(t) + \hat{H}^*(t) - F(t). \tag{12}$$

Substituting (8) and (10) into (7) yields the control law of DOB

$$\begin{aligned} F(t) &= \hat{D}^*(t)V(t) + \hat{H}^*(t) - \hat{F}_{ud}(t-T) \\ &= \hat{D}^*(t)V(t) + \hat{H}^*(t) - (F_{est}(t-T) - F(t-T)). \end{aligned} \tag{13}$$

Substituting the delayed version of (11) into (13) yields the eventual control law

$$\begin{aligned} F(t) = \hat{D}^*(t)V(t) - \hat{D}^*(t-T)\ddot{X}(t-T) \\ + \hat{H}^*(t) - \hat{H}^*(t-T) + F(t-T). \end{aligned} \tag{14}$$

Therefore, if the sampling time is sufficiently fast that $t \approx t - T$, then the following can be assumed:

$$\hat{D}^*(t) \approx \hat{D}^*(t-T), \hat{H}^*(t) \approx \hat{H}^*(t-T), F(t) \approx F(t-T). \tag{15}$$

Then we can achieve the following relationship from (14):

$$\hat{D}^*(t)(V(t) - \ddot{X}(t-T)) = 0. \tag{16}$$

Substituting (6) into (16) yields the decoupled closed-loop error equation for realizing independent axis control

$$\hat{D}^*(t)(\ddot{e}(t) + K_D\dot{e}(t) + K_Pe(t)) = 0, \tag{17}$$

where $\ddot{X}(t) \approx \ddot{X}(t-T)$ is assumed.

Fig.1 shows the corresponding control block diagram of the model–based nonlinear DOB in Cartesian space.

B. NONMODEL-BASED DISTURBANCE OBSERVER

For the nonmodel-based nonlinear DOB, we do not use any models; hence, we set the inertia matrix estimate $\hat{D}^*(t)$ to a constant inertia matrix $\bar{D}^*$ and eliminate the model $\hat{H}^*(t)$ from Fig. 1. The nonmodel-based nonlinear DOB control law from (13) becomes

$$\begin{aligned} F(t) &= \bar{D}^*V(t) - \hat{F}_{ud}(t-T) \\ &= \bar{D}^*V(t) - (F_{est}(t-T) - F(t-T)), \end{aligned} \tag{18}$$

where the model estimate $F_{est}(t)$ becomes the product of a constant inertia matrix and the acceleration signal

$$F_{est}(t) = \bar{D}^*\ddot{X}(t), \tag{19}$$

where $\bar{D}^* = \alpha^* I$ and α^* is a constant.

Substituting the delayed version of (19) into (18) yields the nonmodel-based nonlinear DOB control law

$$F(t) = \bar{D}^*V(t) - \bar{D}^*\ddot{X}(t-T) + F(t-T) \tag{20}$$

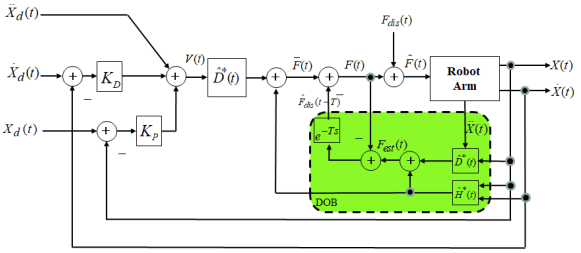

FIGURE 1. Model-based nonlinear DOB control structure.

To implement (20), we require a constant inertia matrix $\bar{D}^*$, a delayed acceleration signal $\ddot{X}(t-T)$, and a previous control law $F(t-T)$. Fig. 2 shows a control block diagram of the nonmodel-based nonlinear DOB.

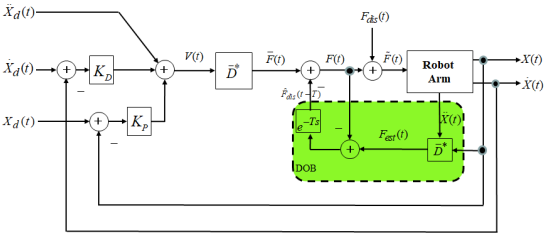

FIGURE 2. Nonmodel-based nonlinear DOB control structure.

The complete control law becomes

$$F(t) = \bar{D}^*(\ddot{X}_d(t) + K_D\dot{e}(t) + K_Pe(t)) - \bar{D}^*\ddot{X}(t-T) + F(t-T) \tag{21}$$

This is known as the time-delayed control which is described in next section.

IV. TIME-DELAYED CONTROL

A. TDC SCHEME

From (4), the Cartesian dynamics for TDC can be described as

$$D^*(t)\ddot{X}(t) + \bar{H}^*(t) = F(t), \tag{22}$$

where $\bar{H}^*(t) = H^*(t) + F_u(t) - F_d(t)$, which includes all the dynamics except an inertia force.

The main strategy of TDC is to estimate $\bar{H}^*(t)$ from (22) as

$$\bar{H}^*(t) = F(t) - \hat{D}^*(t)\ddot{X}(t). \tag{23}$$

Since $\bar{H}^*(t)$ is not available at the same sampling time, it can be obtained by using the previously sampled information as

$$\hat{\bar{H}}^*(t) = \bar{H}^*(t-T) = F(t-T) - \hat{D}^*(t-T)\ddot{X}(t-T), \tag{24}$$

where T is the one sample time delay. Then, a new TDC law is established as

$$\begin{aligned} F(t) &= \hat{D}^*(t)V(t) + \hat{\bar{H}}(t) \\ &= \hat{D}^*(t)V(t) + F(t-T) - \hat{D}^*(t-T)\ddot{X}(t-T). \end{aligned} \tag{25}$$

Substituting (6) into (25) yields the TDC control law

$$\begin{aligned} F(t) = \hat{D}^*(t)(\ddot{X}_d(t) + K_D\dot{e}(t) + K_Pe(t)) + F(t-T) \\ - \hat{D}^*(t-T)\ddot{X}(t-T). \end{aligned} \tag{26}$$

If we use the constant inertia matrix $\bar{D}^*$ instead of $\hat{D}^*(t)$ and $\hat{D}^*(t-T)$ in (26) then the control law becomes model free.

$$F(t) = \bar{D}^*(\ddot{X}_d(t) + K_D\dot{e}(t) + K_P e(t)) + F(t-T) - \bar{D}^*\ddot{X}(t-T). \quad (27)$$

According to careful examination of (27), $\bar{D}^*, \ddot{X}(t-T)$ and the fast sampling time T are required to realize the TDC scheme.

Comparing the TDC control law in (27) with the nonmodel-based nonlinear DOB control law in (21), the two schemes eventually become the same; hence, the structure of TDC is equivalent to that of the nonmodel-based nonlinear DOB.

Another important consideration in Cartesian space control is the transformation from the Cartesian force to the joint torque, which can be realized by applying the Jacobian relation as follows:

$$\tau(t) = J^T F(t). \quad (28)$$

Fig. 3 shows a TDC block diagram, which eventually becomes the same as the diagram in Fig. 2.

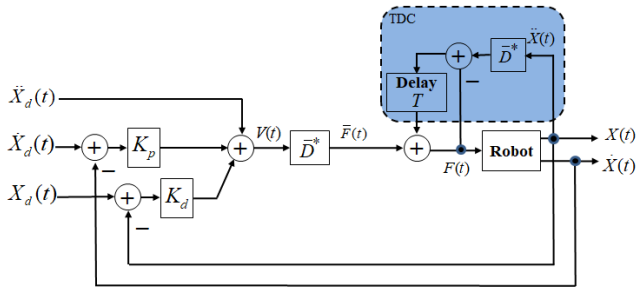

FIGURE 3. TDC structure.

B. STABILITY ANALYSIS

Acceleration signals $\ddot{X}(t)$ are important for extracting the uncertain dynamics information in both the DOB and TDC schemes. Combining (22) and (25) yields the acceleration error as in (16), which is defined as

$$\zeta(t) = \ddot{X}(t) - V(t). \quad (29)$$

Multiplying both sides of (29) by $D^*(t)$ and substituting $\ddot{X}(t)$ from the Cartesian dynamic equation (22) yields

$$\begin{aligned} D^*(t)\zeta(t) &= D^*(t)[D^{*-1}(t)(F(t) - \bar{H}^*(t)) - V(t)] \\ &= F(t) - \bar{H}^*(t) - D^*(t)V(t). \end{aligned} \quad (30)$$

Substituting $F(t)$ with the Cartesian TDC law (27) into (30) yields

$$\begin{aligned} D^*(t)\zeta(t) &= \bar{D}^*V(t) + F(t-T) - \bar{D}^*\ddot{X}(t-T) \\ &\quad -\bar{H}^*(t) - D^*(t)V(t), \end{aligned} \quad (31)$$

Substituting the delayed version $F(t-T)$ of the Cartesian dynamic equation (22) into (31) yields

$$\begin{aligned} D^*(t)\zeta(t) &= \bar{D}^*V(t) + D^*(t-T)\ddot{X}(t-T) + \bar{H}^*(t-T) \\ &\quad -\bar{D}^*\ddot{X}(t-T) - \bar{H}^*(t) - D^*(t)V(t) \\ &= (\bar{D}^* - D^*(t))V(t) + (D^*(t-T) - \bar{D}^*)\ddot{X}(t-T) \\ &\quad +\bar{H}^*(t-T) - \bar{H}^*(t), \end{aligned} \quad (32)$$

Dividing both side of (32) by $D^*(t)$ yields

$$\begin{aligned} \zeta(t) &= (D^{*-1}(t)\bar{D}^* - I)V(t) + D^{*-1}(t)(D^*(t-T) - \bar{D}^*) \\ &\quad \times \ddot{X}(t-T) + D^{*-1}(t)(\bar{H}^*(t-T) - \bar{H}^*(t)), \end{aligned} \quad (33)$$

Substituting $\ddot{X}(t-T) = V(t-T) + \zeta(t-T)$ from (29) into (33) yields

$$\begin{aligned} \zeta(t) &= -(I - D^{*-1}(t)\bar{D}^*)V(t) + D^{*-1}(t)(D^*(t-T) - \bar{D}^*) \\ &\quad \times V(t-T) + D^{*-1}(t)(D^*(t-T) - \bar{D}^*)\zeta(t-T)) \\ &\quad + D^{*-1}(t)(\bar{H}^*(t-T) - \bar{H}^*(t)), \end{aligned} \quad (34)$$

Adding and subtracting $\zeta(t-T)$ and rearranging (34) yields

$$\begin{aligned} \zeta(t) &= -(I - D^{*-1}(t)\bar{D}^*)V(t) + D^{*-1}(t)(D^*(t-T) - \bar{D}^*) \\ &\quad \times V(t-T) + (I - D^{*-1}(t)\bar{D}^*)\zeta(t-T) \\ &\quad - (I - D^{*-1}(t)D^*(t-T))\zeta(t-T) \\ &\quad + D^{*-1}(t)(\bar{H}^*(t-T) - \bar{H}^*(t)), \end{aligned} \quad (35)$$

Substituting $\zeta(t-T) = \ddot{X}(t-T) - V(t-T)$ from (29) into (35) yields

$$\begin{aligned} \zeta(t) &= [I - D^{*-1}(t)\bar{D}^*]\zeta(t-T) + [I - D^{*-1}(t)\bar{D}^*] \\ &\quad (V(t-T) - V(t)) - [I - D^{*-1}(t)D^*(t-T)] \\ &\quad \ddot{X}(t-T) + D^{*-1}(t)[\bar{H}^*(t-T) - \bar{H}^*(t)], \end{aligned} \quad (36)$$

Rearranging (36) by defining the forcing function $r(t)$ yields

$$\zeta(t) = [I - D^{*-1}(t)\bar{D}^*]\zeta(t-T) + r(t), \quad (37)$$

where $D^*(t)$ is the Cartesian inertia matrix and $\bar{D}^*$ is the Cartesian constant inertia matrix. The forcing function is defined as

$$\begin{aligned} r(t) &= [I - D^{*-1}(t)\bar{D}^*](V(t-T) - V(t)) - [I - D^{*-1}(t) \\ &\quad D^*(t-T)]\ddot{X}(t-T) + D^{*-1}[\bar{H}^*(t-T) - \bar{H}^*(t)]. \end{aligned} \quad (38)$$

According to careful examination of (38), the forcing function $r(t)$ can be zero if the sampling time is sufficiently fast such that $V(t) \approx V(t-T)$, $D^*(t) \approx D^*(t-T)$, and $\bar{H}^*(t) \approx \bar{H}^*(t-T)$.

Then (37) becomes a first order delayed equation

$$\zeta(t) - [I - D^{*-1}(t)\bar{D}^*]\zeta(t-T) = 0. \quad (39)$$

In the discrete domain, (39) can be represented as a first order difference equation

$$\zeta(k) - [I - D^{*-1}(k)\bar{D}^*]\zeta(k-1) = 0. \quad (40)$$

For the stability condition of the Cartesian TDC in the discrete domain, the stability bound is

$$||I - D^{*-1}(k)\bar{D}^*|| < 1, \quad (41)$$

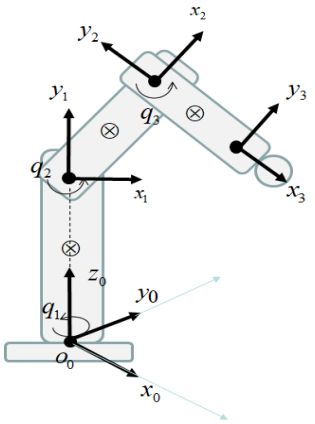

FIGURE 4. Environment setup.

TABLE 1. Specifications of a robot manipulator.

	Joint 1	Joint 2	Joint 3
Initial angle(rad)	$\frac{\pi}{4}$	$\frac{\pi}{4}$	$-\frac{\pi}{2}$
Mass(kg)	10	3	3
Length(m)	0.5	0.3	0.3
Frictions	$0.5\text{sgn}(\dot{q})+0.3\dot{q}$	$0.5\,\text{sgn}(\dot{q})+0.3\dot{q}$	$0.5\,\text{sgn}(\dot{q})+0.3\dot{q}$

Thus, the constant inertia value $\bar{D}^*$ should be selected to satisfy the stability condition (41) for the stable control response.

V. NUMERICAL STUDIES

A. SIMULATION SETUP

Fig. 4 illustrates a three-link robot that is initially located at $X_0 = [0.3, 0.3, 0.5]^T m$ for evaluation of the position tracking performance. The initial angle of the robot is $q_0 = [\pi/4, \pi/4\ , -\pi/2]^T$. It is assumed that each joint has nonlinear friction $0.5sgn(\dot{q}) + 0.3\dot{q}$.

Table 1 lists the parameters of the robot. The robot is required to follow a circular trajectory with a radius of $0.2m$ that is configured in the xyz-plane so that the robot is controlled in all the axes. Position control tasks for the sampling times of 0.01s and 0.001s are conducted for comparison.

First, we evaluate several control schemes under nonmodel dynamics with joint frictions. Joint torques are bounded by $\pm 50Nm$ for the actuator protection.

As a performance measure, the root-mean-squared (RMS) error of the tracking of a complete circular trajectory is calculated for the performance comparison of each control scheme.

$$p_{error} = \sqrt{\sum((x_d - x)^2 + (y_d - y)^2 + (z_d - z)^2)} \quad (42)$$

B. CARTESIAN PD CONTROL

In the first test, the PD control scheme is used to control a robot to follow the circular trajectory. Controller gains are selected as, $K_D = 20I$, $K_P = 100I$. Table 2 lists the RMS tracking errors for various torque constants. Fig. 5 shows the tracking results for various torque matrices, $K_T = k_T I$. The best performance is realized when $k_T = 21$, but the tracking performance remains poor as shown in Fig. 5(b).

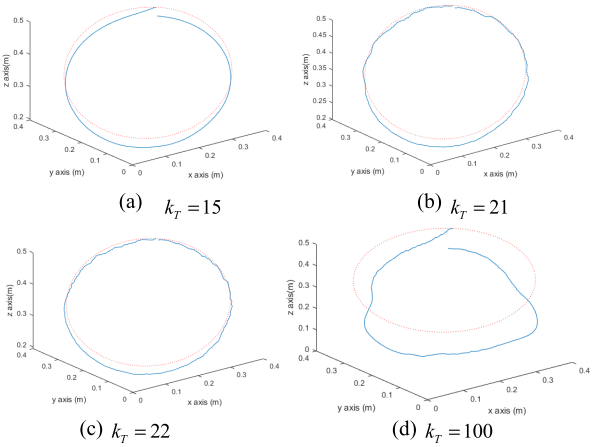

FIGURE 5. PD control performance.

TABLE 2. RMS errors for various torque constants.

	$k_T=1$	$k_T=10$	$k_T=15$	$k_T=18$	$k_T=19$	$k_T=20$
RMS error	7.3132	3.4767	0.7383	0.6432	0.6305	0.6257
	$k_T=21$	$k_T=22$	$k_T=25$	$k_T=30$	$k_T=50$	$k_T=100$
RMS error	**0.6236**	0.6441	1.4338	1.6152	2.0883	2.3976

Even though the gain is increased, the tracking performance was not improved due to the torque saturation and nonlinear joint frictions as shown in Fig. 5 (d).

It is difficult for the PD control scheme to find a suitable torque constant to minimize the Cartesian position tracking errors; hence, the Cartesian PD control scheme seldom satisfies the tracking performance requirements. In most cases, full dynamic models are not available, and additional uncertainties are present. As a result, the performances of PD control are degraded, as listed in Table 2.

C. CARTESIAN TDC SCHEME

Next, the TDC scheme for the same circular trajectory tracking task is evaluated. Two sampling times, namely, $T = 0.001s$ and $T = 0.01$s, are tested.

1) CASE 1: $T = 0.001s$ AND $k_T = 1$

We begin with the constant inertia $\alpha^* = 0.01$, which results in an unstable response. As the inertia value is increased gradually, the tracking error decreases. However, joint torques start oscillating. Fig. 6 shows the circular trajectory tracking results for $\alpha^* = 0.05$, 1.1, 1.2, and 1.5. The tracking performances for $\alpha^* = 1.1$, 1.2, and 1.5 are comparable, whereas that for $\alpha^* = 0.05$ is not. Table 3 lists the RMS errors of the circular trajectory tracking for various values of α^*. Here the torque is set to a constant value of 1.

However, the joint torques with $\alpha^* = 1.2$ exhibit chattering behavior as shown in Fig. 7 (b). As the constant inertia value is increased, the position tracking errors remain similar, but severely chattering torques are observed. Thus, we select $\alpha^* = 1.1$ to realize the best performance, as listed in Table 3.

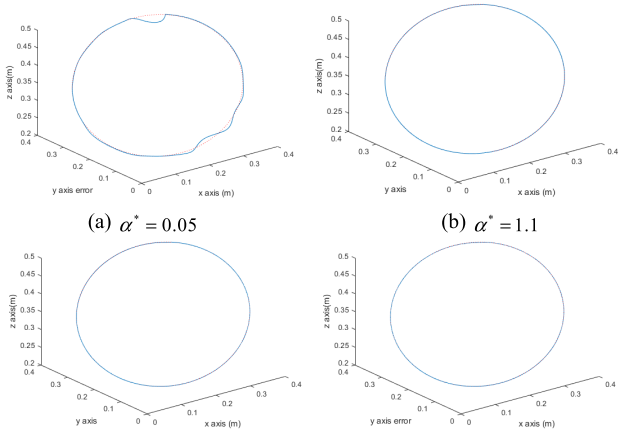

(a) $\alpha^* = 0.05$ (b) $\alpha^* = 1.1$ (c) $\alpha^* = 1.2$ (d) $\alpha^* = 1.5$

FIGURE 6. TDC tracking performance when T=0.001s and $k_T = 1$.

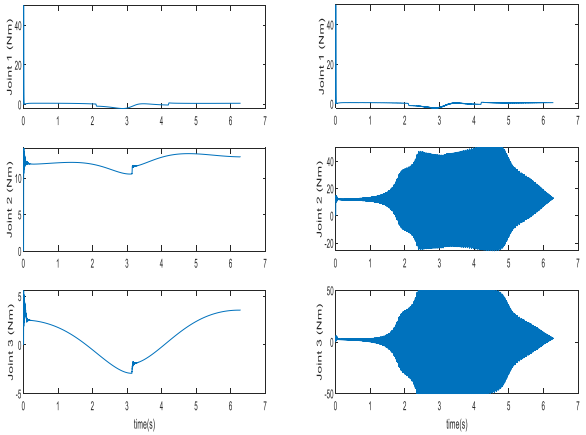

(a) $\alpha^* = 1.1$ (b) $\alpha^* = 1.2$

FIGURE 7. Joint torques when T=0.001s.

TABLE 3. RMS errors for various inertia values when $T = 0.001s$ and $k_T = 1$.

	$\alpha^* = 0.01$	$\alpha^* = 0.1$	$\alpha^* = 0.3$	$\alpha^* = 0.5$	$\alpha^* = 0.8$	$\alpha^* = 0.9$
RMS error	Unstable	0.2454	0.0720	0.0427	0.0267	0.0238
	$\alpha^* = 1.0$	$\alpha^* = 1.1$	$\alpha^* = 1.2$	$\alpha^* = 1.3$	$\alpha^* = 1.4$	$\alpha^* = 1.5$
RMS error	0.0215	**0.0197**	0.0190	0.0196	0.0218	0.0230

A reasonable bound for the inertia value for the tracking performance was identified by simulation studies as $0.03 \leq \alpha^* \leq 1.1$.

2) CASE 2: $T = 0.001s$ AND $k_T = 10$

We increased the torque constant to 10. Fig. 8 shows the corresponding performances and Table 4 lists the RMS position tracking errors for various inertia values. Above $\alpha^* = 1.1$, the joint torques show chattering behaviors. Therefore, the best performance is realized when $\alpha^* = 0.5$ in Table 4, and the error exceeds that for $\alpha^* = 1.1$ when $k_T = 1$ is used, as presented in Table 3.

We have identified the stable region of the inertia value as $0.02 \leq \alpha^* < 1.1$. The overall tracking errors exceed those

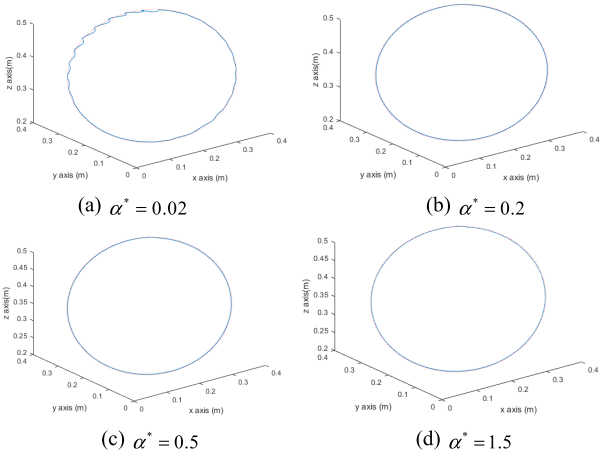

(a) $\alpha^* = 0.02$ (b) $\alpha^* = 0.2$ (c) $\alpha^* = 0.5$ (d) $\alpha^* = 1.5$

FIGURE 8. TDC tracking performance when T=0.001s and $k_T = 10$.

TABLE 4. RMS errors for various inertia values when $T = 0.001s$ and $k_T = 10$.

	$\alpha^* = 0.01$	$\alpha^* = 0.02$	$\alpha^* = 0.03$	$\alpha^* = 0.05$	$\alpha^* = 0.1$	$\alpha^* = 0.2$
RMS error	Unstable	0.3137	0.2286	0.1851	0.1684	0.1650
	$\alpha^* = 0.5$	$\alpha^* = 0.7$	$\alpha^* = 0.9$	$\alpha^* = 1.0$	$\alpha^* = 1.1$	$\alpha^* = 1.2$
RMS error	**0.1642**	0.1642	0.1642	0.1642	0.1643	0.1643

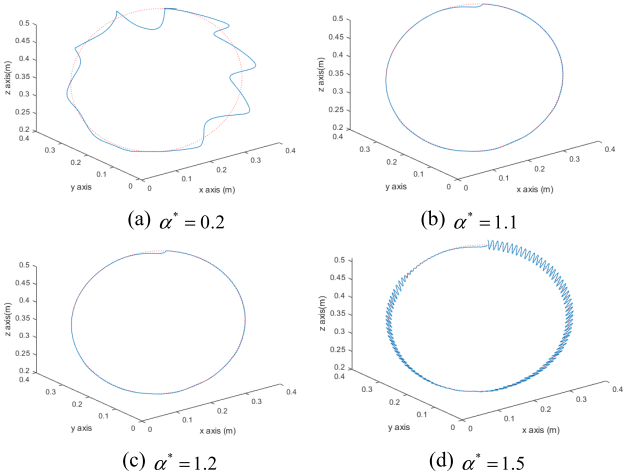

(a) $\alpha^* = 0.2$ (b) $\alpha^* = 1.1$ (c) $\alpha^* = 1.2$ (d) $\alpha^* = 1.5$

FIGURE 9. TDC tracking performance when T=0.01s.

in Case 1. Hence, higher torque gains do not always improve the tracking performance, even under the fast sampling time. The simulation results also suggest that the use of the torque constant is unnecessary when the sampling time is fast, such as $T = 0.001s$.

3) CASE 3: $T = 0.01s$ AND $k_T = 1$

For the slower sampling time $T = 0.01s$, the overall performances of the TDC scheme, which are presented in Fig. 9, are lower than those with $T = 0.001s$, which are presented in Fig. 6. A reasonable bound on the tracking performance was identified by simulation studies to be $0.2 \leq \alpha^* \leq 1.1$, as listed in Table 5. However, when the inertia value exceeds $\alpha^* = 1.3$, the trajectory tracking response chatters, as shown

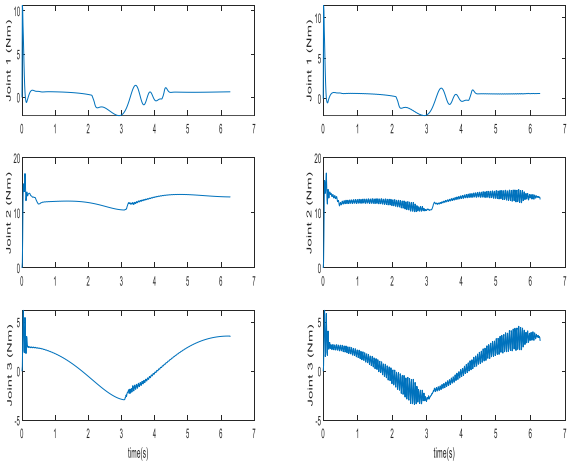

(a) $\alpha^* = 1.1$ (b) $\alpha^* = 1.2$

FIGURE 10. Joint torques when T=0.01s.

TABLE 5. RMS errors for various inertia values when $T = 0.01s$ and $k_T = 1$.

	$\alpha^*=0.1$	$\alpha^*=0.2$	$\alpha^*=0.3$	$\alpha^*=0.5$	$\alpha^*=0.8$	$\alpha^*=0.9$
RMS error	Unstable	0.7050	0.3066	0.1721	0.0970	0.0841
	$\alpha^*=1.0$	$\alpha^*=1.1$	$\alpha^*=1.2$	$\alpha^*=1.3$	$\alpha^*=1.4$	$\alpha^*=1.5$
RMS error	0.0743	**0.0666**	0.0605	0.0551	0.2127	0.2408

TABLE 6. RMS errors for various inertia values when $T = 0.01s$ and $k_T = 10$.

	$\alpha^*=0.1$	$\alpha^*=0.2$	$\alpha^*=0.3$	$\alpha^*=0.5$	$\alpha^*=0.8$	$\alpha^*=0.9$
RMS error	0.1452	0.0677	0.0555	0.0496	0.0468	**0.0460**
	$\alpha^*=1.0$	$\alpha^*=1.1$	$\alpha^*=1.2$	$\alpha^*=1.3$	$\alpha^*=1.4$	$\alpha^*=1.5$
RMS error	0.0446	0.0464	0.0631	0.3164	0.8919	0.8100

in Fig. 9 (b). The joint torques also chatter as shown in Fig. 10 (b). Fig. 11 shows the tracking error for each axis when $\alpha^* = 1.1$, which is considered to be the optimal value.

4) CASE 4: $T = 0.001s$ AND $k_T = 10$

The tracking performance can be further improved by increasing the torque constant to $k_T = 10$. Table 6 lists the RMS errors for various values of α^*. A reasonable bound on the inertia value for the tracking performance is identified by simulation studies to be $0.1 \leq \alpha^* \leq 1.1$, which is similar to that in Case 3. The overall tracking errors are lower than those of Case 3; hence, the higher torque constant is required to improve the tracking control performance when the sampling time is not sufficiently fast.

D. SUMMARY OF THE SIMULATION RESULTS

1) COMPARISON STUDIES

We have listed the best performance and the stability region for each of the four cases in Table 7. The lower limit of α^* is selected when the robot can follow the circular trajectory

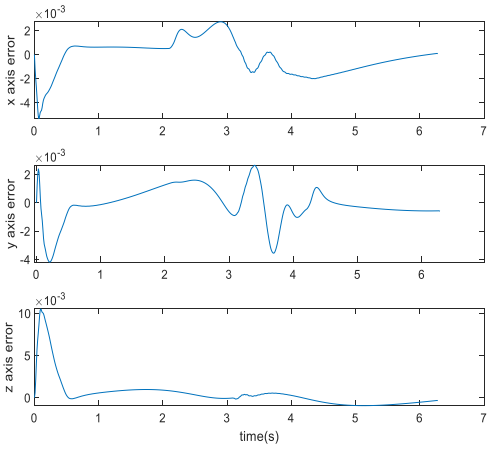

FIGURE 11. Axis tracking error of $\alpha^* = 1.1$ when T=0.01s.

TABLE 7. Summary of all cases.

	Case 1 $T=0.001s$ $k_T=1$	Case 2 $T=0.001s$ $k_T=10$	Case 3 $T=0.01s$ $k_T=1$	Case 4 $T=0.01s$ $k_T=10$
Best α^*	1.1	1.0	1.1	0.9
RMS Error	0.0197	0.1642	0.0666	0.0460
Stability Region	$0.03 \leq \alpha^* \leq 1.1$	$0.02 \leq \alpha^* < 1.1$	$0.2 \leq \alpha^* \leq 1.1$	$0.1 \leq \alpha^* \leq 1.1$

TABLE 8. RMS errors for various inertia values when $T = 0.001s$ and $\alpha^* = 1$.

	$k_T=0.5$	$k_T=1$	$k_T=1.5$	$k_T=2$
RMS Error	0.1930	**0.0215**	0.0599	0.0891

from unstable states and the upper limit of α^* is defined just before chattering behaviors start.

An interesting observation is that the lower and upper limits are approximately the same for the same sampling time. The upper limit is approximately the same for all the cases. Therefore, there exists a stability bound as described in (41).

2) PERFORMANCE EVALUATION WITH VARIOUS TORQUE CONSTANTS

For each sampling time, the effects of the torque constant k_T on the tracking performance have been evaluated. The inertia value is set to $\alpha^* = 1$ for all cases. Table 8 lists the RMS errors for various k_T values with the sampling time of $T = 0.001s$. The best tracking performance is realized when $k_T = 1$. When the higher torque gain is used, the lower performance is observed. Hence, tuning the torque constant is unnecessary with a fast sampling time, such as $T = 0.001s$.

For the sampling time $T = 0.01s$, interesting results have been obtained as listed in Table 9. A superior tracking response is observed when the torque constant is $k_T = 3$ compared to $k_T = 1$; thus, the torque constant must be increasingly optimized for the slower sampling time. The increased tracking error is also caused by the slow sampling time.

TABLE 9. RMS errors for various inertia values when $T = 0.01s$ and $\alpha^* = 1$.

	$k_T = 0.5$	$k_T = 1$	$k_T = 1.5$	$k_T = 2$	$k_T = 3$	$k_T = 5$
RMS Error	0.1687	0.0743	0.0496	0.0420	**0.0401**	0.0429

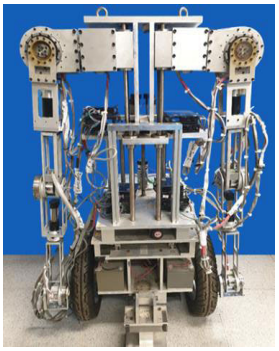

FIGURE 12. Two arm mobile manipulator.

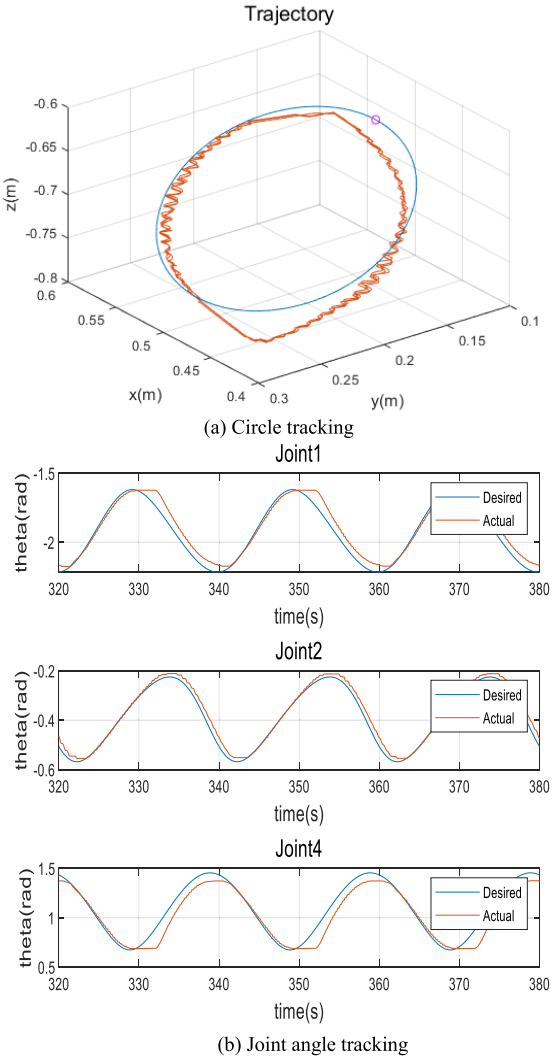

FIGURE 13. Tracking results of PD control.

VI. EXPERIMENTAL STUDIES

Here, we obtain experimental results for comparison with the simulation results.

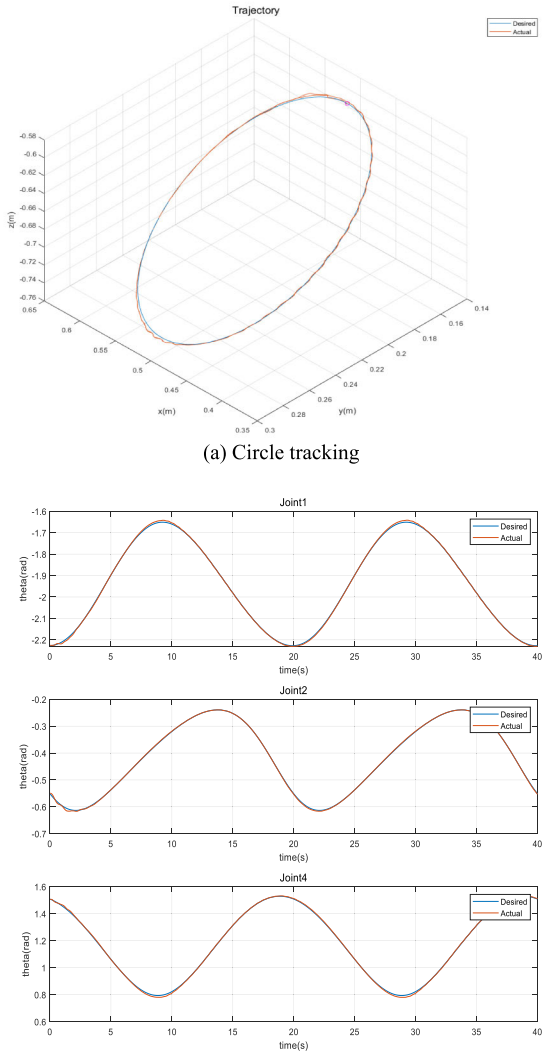

FIGURE 14. Tracking results of TDC.

A. EXPERIMENTAL SETUP

The test-bed is a mobile manipulator that was built in our laboratory as shown in Fig. 12. It has two arms with 6 degrees of freedom and two wheels. The first three links are controlled to follow the circular trajectory. The sampling time is $T = 0.01s$.

B. PD CONTROL SCHEME

Fig. 13 shows the tracking response that was obtained using a PD control scheme. We observe the notable tracking error with chattering behaviors due to high gain effects. The controller gains were $K_P = [18000, 17000, 16000]^T$, and $K_D = [2000, 2000, 1000]^T$. The torque constants was $K_T = [21, 21, 10]^T$. The high gains of the PD control scheme did not satisfy the performance requirements.

C. TDC SCHEME

The same task was performed by the TDC scheme. Fig. 14 shows the better tracking response. The tracking

errors were reduced even when smaller gains were used. The controller gains were $K_P = [600, 500, 400]^T$ and $K_D = [60, 50, 40]^T$. The inertia constant was $\alpha^* = 1.5$, and the torque constant vector was $K_T = [2.8, 2.7, 2.6]^T$. The RMS error of Fig. 14 (a) is 0.0841.

VII. CONCLUSION

In this paper, we have shown that the time-delayed control method eventually becomes equivalent to a nonmodel-based nonlinear disturbance observer. Numerical and experimental studies have shown that PD controllers exhibit limited performances due to nonlinear uncertainties in robot manipulators. Superior performance by TDC was observed when the constant inertia matrix was suitably selected within the stability bound. However, the selection of an unsuitable constant inertia matrix resulted in poor tracking performance and even instability. We also considered two sampling times. As expected, the tracking performances at the faster sampling time were superior; thus, the sampling time is important in TDC. For the low sampling time, the torque constant can be used to improve the position tracking performance. The upper limit of the constant inertia is almost same for all the cases. Although the stability bound in (41) is approximated in a discrete domain, consistency of the stability bounds has been observed in numerical studies. Empirical results demonstrate the outperformance by TDC scheme.

REFERENCES

[1] M. Tomizuka, "Robust digital motion controllers for mechanical systems," *Robot. Auton. Syst.*, vol. 19, no. 2, pp. 143–149, 1996.

[2] K. Kim and D. Hong, "Robotic biceps exercise machine: Hardware using series elastic actuator and control with disturbance observer," *IEEE Access*, vol. 8, pp. 12758–12767, 2020.

[3] W.-H. Chen, D. J. Ballance, P. J. Gawthrop, and J. O'Reilly, "A nonlinear disturbance observer for robotic manipulators," *IEEE Trans. Ind. Electron.*, vol. 47, no. 4, pp. 932–938, Aug. 2000.

[4] K. Kong and M. Tomizuka, "Nominal model manipulation for enhancement of stability robustness for disturbance observer-based control systems," *Int. J. Control, Automat. Syst.*, vol. 11, no. 1, pp. 12–20, 2013.

[5] Y.-J. Ko, Y.-J. Kim, and J.-S. Kim, "Robust speed control of an autonomous vehicle using disturbance observer," *J. Inst. Control, Robot. Syst.*, vol. 22, no. 5, pp. 339–345, May 2016.

[6] I. H. Kim and Y. I. Son, "Design of a DC motor current controller using a sliding mode disturbance observer and controller," *J. Inst. Control, Robot. Syst.*, vol. 22, no. 6, pp. 417–423, Jun. 2016.

[7] A. Mohammadi, H. J. Marquez, and M. Tavakoli, "Nonlinear disturbance observers: Design and applications to Euler–Lagrange systems," *IEEE Control Syst. Mag.*, vol. 37, no. 4, pp. 50–72, Aug. 2017.

[8] J.-S. Kim and J. Back, "Practical stabilization of an uncertain linear systems using state feedback based disturbance observer," *J. Inst. Control, Robot. Syst.*, vol. 23, no. 11, pp. 942–947, Nov. 2017.

[9] Z.-J. Yang, Y. Fukushima, and P. Qin, "Decentralized adaptive robust control of robot manipulators using disturbance observers," *IEEE Trans. Control Syst. Technol.*, vol. 20, no. 5, pp. 1357–1365, Sep. 2012.

[10] H. Gomi and M. Kawato, "Learning control for a closed loop system using feedback-error-learning," in *Proc. 29th IEEE Conf. Decis. Control*, Dec. 1990, pp. 3289–3294.

[11] F. L. Lewis, S. Jagannathan, and A. Yesildirek, *Neural Network Control of Robot Manipulators and Nonlinear Systems*. London, U.K.: Taylor & Francis, 1999.

[12] S. Jung and T. C. Hsia, "Neural network inverse control techniques for PD controlled robot manipulator," *Robotica*, vol. 18, no. 3, pp. 305–314, May 2000.

[13] C. G. Yang, Z. Li, R. Cui, and B. Xu, "Neural network-based motion control of an underactuated wheeled inverted pendulum model," *IEEE Trans. Neural Netw. Learn. Syst.*, vol. 25, no. 11, pp. 2004–2016, Nov. 2014.

[14] S. Li, Y. Zhang, and L. Jin, "Kinematic control of redundant manipulators using neural networks," *IEEE Trans. Neural Netw. Learn. Syst.*, vol. 28, no. 10, pp. 2243–2254, Oct. 2017.

[15] S. Jung, "A neural network technique of compensating for an inertia model error in a time-delayed controller for robot manipulators," *Int. J. Control, Autom. Syst.*, vol. 18, no. 7, pp. 1863–1871, Jul. 2020.

[16] J. Guan, C.-M. Lin, G.-L. Ji, L.-W. Qian, and Y.-M. Zheng, "Robust adaptive tracking control for manipulators based on a TSK fuzzy cerebellar model articulation controller," *IEEE Access*, vol. 6, pp. 1670–1679, 2018.

[17] H. Hu, X. Wang, and L. Chen, "Impedance sliding mode control with adaptive fuzzy compensation for robot-environment interacting," *IEEE Access*, vol. 8, pp. 19880–19889, 2020.

[18] Y. Liu and Q. Zhu, "Adaptive fuzzy finite-time control for nonstrict-feedback nonlinear systems," *IEEE Trans. Cybern.*, early access, Mar. 23, 2021, doi: 10.1109/TCYB.2021.3063139.

[19] R. Morgan and U. Ozguner, "A decentralized variable structure control algorithm for robotic manipulators," *IEEE J. Robot. Autom.*, vol. 1, no. 1, pp. 57–65, Mar. 1985.

[20] T. Hsia, "On a simplified joint controller design for robot manipulators," in *Proc. 26th IEEE Conf. Decis. Control*, Dec. 1987, pp. 1024–1025.

[21] K. Youcef-Toumi and O. Ito, "A time-delay controller for systems with unknown dynamics," *J. Dyn. Syst., Meas., Control*, vol. 112, no. 1, pp. 133–142, 1990.

[22] S. Jung, T. C. Hsia, and R. G. Bonitz, "Force tracking impedance control of robot manipulators under unknown environment," *IEEE Trans. Control Syst. Technol.*, vol. 12, no. 3, pp. 474–483, May 2004.

[23] P. H. Chang and S. H. Park, "On improving time-delay control under certain hard nonlinearities," *Mechatronics*, vol. 13, no. 4, pp. 393–412, May 2003.

[24] S.-U. Lee and P. H. Chang, "The development of anti-windup scheme for time delay control with switching action using integral sliding surface," *J. Dyn. Syst., Meas., Control*, vol. 125, no. 4, pp. 630–638, Dec. 2003.

[25] J. Baek, W. Kwon, B. Kim, and S. Han, "A widely adaptive time-delayed control and its application to robot manipulators," *IEEE Trans. Ind. Electron.*, vol. 66, no. 7, pp. 5332–5342, Jul. 2019.

[26] J. Lee, P. H. Chang, and M. Jin, "An adaptive gain dynamics for time delay control improves accuracy and robustness to significant payload changes for robots," *IEEE Trans. Ind. Electron.*, vol. 67, no. 4, pp. 3076–3085, Apr. 2020.

SEUL JUNG (Member, IEEE) received the B.S. degree in electrical and computer engineering from Wayne State University, Detroit, MI, USA, in 1988, and the M.S. and Ph.D. degrees in electrical and computer engineering from the University of California at Davis, in 1991 and 1996, respectively. In 1997, he joined the Department of Mechatronics Engineering, Chungnam National University, South Korea, where he is presently a Professor. His research interests include intelligent mechatronics systems, intelligent robotic systems, mobile manipulators for home service applications, gyroscope applications, and robot education. He is a member of ACA, ICROS, KROS, KIIS, KIEE, IEMEK, and IEEK. He is the General Co-Chair of ICCAS 2021.

JOON WOO LEE received the B.S. degree in electrical engineering from Korea National University of Transportation, in 2019. He is currently a Graduate Student with the Department of Mechatronics Engineering, Chungnam National University, Daejeon, South Korea. His research interests include robot manipulator control, robot manipulator applications, and control moment gyroscope control.